Journal of Environment & Biotechnology Research
VINANIE PUBLISHERS
www.vinanie.com/jebr

Synergism and activity enhancement in new photocatalysts derived from zeolite, tungsten trioxide and polyaniline leading to visible light destruction of p-nitrophenol

A. Bala Nambi, J.V. Anusha, E. Subramanian*

Department of Chemistry, Manonmaniam Sundaranar University, Tirunelveli, India

ORIGINAL RESEARCH ARTICLE

ABSTRACT

Synthesis of single (zeolite-HX), binary (WO_3/zeolite-HX, zeolite-HX/PANI) and ternary (WO_3/zeolite-HX/PANI) photocatalysts was performed involving zeolite as adsorbent, WO_3 as semiconductor and polyaniline (PANI) as visible light sensitizer. Zeolite-HX was obtained from coal fly ash by alkali fusion followed by hydrothermal treatment and the binary and ternary photocatalysts from the precursors of sodium tungstate and aniline monomer. The synthesized catalysts were analysed by Fourier transform infrared, X-ray fluorescence, X-ray diffraction, scanning electron microscopy, energy dispersive X-ray spectroscopy and diffuse reflectance spectroscopy techniques which revealed the physico-chemical characteristics and nanoparticles structures. Photocatalytic destruction of 20 mg/L p-nitrophenol (p-NP) over the synthesized photocatalysts was investigated with visible light irradiation (60 W tungsten lamp) in the presence of H_2O_2. About 3-fold increase in activity from single to binary and a 2-fold increase from binary to ternary system were observed. Among the components, the activity enhancement was in the following order, zeolite < WO_3 < PANI. Around, 20 mg/L p-NP was decolorized through destruction over WO_3/zeolite-HX/PANI within a reaction time of 3 h. Thus the present work has developed an efficient ternary photocatalytic system involving synergism and co-activation.

KEYWORDS

p-nitrophenol destruction; polyaniline; ternary catalyst; tungsten trioxide; zeolite

1. INTRODUCTION

Fly ash (FA) is a fused residue of clay minerals obtained from coal after burning. The high temperature generated when coal burns in thermal power plants, transforms the clay mineral into a variety of fused fine particles with mainly aluminium silicate content. FA is mainly composed of amorphous aluminosilicate glass, crystalline phases (such as quartz, mullite, hermatite, lime and magnetite) together with varying amounts of iron, sodium, potassium, calcium, titanium, sulphur, carbon and manganese oxides (Wang and Wu, 2006; Querol et al., 1995). Coal fly ash is a major solid waste from coal-firing power stations. In India, more than 112 million tons of fly ash is generated every year and the value tends to increase every year (Wang and Wu, 2006; Emamul, 2013). Considering that only about 20-30% of the generated fly ash is used as an additive in cement and concrete manufacture, the management of fly ash is a global concern from both environmental and economic points of view. FA is mainly disposed as land-fill; hence heavy metals present in FA can potentially leach into ground water/water bodies. Being light weight, FA can fly off into air during strong winds and therefore fill the air and atmosphere with dust and particles. The various natural resources (soil, water, and air) thus face pollution threats from FA. Many strategies have been proposed to utilize this waste into useful products (Scheetz and Earle, 1998). Among them, zeolite synthesis is very prominent. Because of high silica and alumina content, fly ash can be converted into zeolite material by hydrothermal treatment, and subsequently it can be used as adsorbents, ion-exchanger, catalyst, etc. (Querol et al.,

Corresponding author: **E. Subramanian**
Tel: +91-9965178458
Fax: +91-462-2334363
E. mail: esubram@yahoo.com

Received: 07-11-2016
Revised: 30-11-2016
Accepted: 15-12-2016
Available online: 01-01-2017

1995; Scheetz and Earle, 1998; Wang and Wu, 2006; Wang, 2008; Klamrassamee et al., 2010; Emamul, 2013).

Zeolites are crystalline nanoporous inorganic materials with well-defined interconnected channels or cavities. With uniform pore size, polar environment, high surface area, internal active sites and excellent adsorption capability (Breck, 1973; Corma and Garcia, 2004), zeolites could enhance the efficiency and selectivity of immobilized photocatalysts by activating them within zeolite framework. Metal oxide semiconductor can be used as a photocatalyst. There are several such photocatalysts, namely TiO_2, ZnO, $SrTiO_3$, Fe_2O_3, etc. (Shinde et al., 2013; Bi and Xu, 2011). WO_3 is a n-type semiconductor material with bandgap energy ranging from 2.6 to 3.0 eV and is stable in acidic medium (Miyauchi, 2008). WO_3 is a multifunctional material used in various applications, namely gas sensors (Ganbavle et al., 2015), photocatalysts (Bi and Xu, 2011; Miyauchi, 2008; Abazari et al., 2014) and electrochromic devices (More et al., 2014). Since WO_3 is a light coloured material, it absorbs visible light with minimal range. Therefore, in order to use WO_3 effectively, it must be sensitized to visible light in a wide range. Hence, WO_3 is modified to a hybrid material with conducting polymer, other metal/non-metal etc., so that the resulting material has wider absorbance in visible light. In the case of conjugated conducting polymers with alternate single and double bonds, they are coloured, absorb visible light and can sensitize photocatalyst like metal oxide semiconductors. Polyaniline (PANI) is a well-known, environmentally stable and highly tunable conducting polymer, which can be produced as bulk powder, cast films and fibers. PANI can facilitate absorption of more visible light and generate more e^--h^+ pair, which could result in the higher photocatalytic activities.

Advanced oxidation process (AOP) is an effective tool to the destruction of a wide range of pollutants, leading to their almost complete mineralization (Thakare, 2004). Photocatalysis is an advanced oxidation process. Photocatalyst generates highly reactive oxygen species ($OH^{\bullet}$, $O_2^{\bullet-}$ etc) which destruct unspecifically all types of organic pollutants. Photocatalysis in solar/visible light is a green method and hence the same is adopted in the present work. The main aim of the present work is the development of single, binary and ternary photocatalyst materials involving zeolite adsorbent, WO_3 semiconductor and polyaniline visible light sensitizer. These photocatalysts were assessed for their visible light activity by the photocatalytic destruction and degradation of p-nitrophenol (p-NP). Phenolic compounds discharged in effluents from petrochemicals, agrochemicals, plastics industries, preservative industries, coal distillation plants, pharmaceutical industries etc., are carcinogenic and harmful to the environment (Mele et al., 2003). Hence p-NP was chosen as the organic pollutant in the present work and a systematic investigation on its visible light photodegradation was performed. Interesting results were obtained demonstrating greater efficiencies and synergism.

2. MATERIALS AND METHODS

2.1. Materials

Coal fly ash sample was obtained from the electrostatic precipitators of Tuticorin Thermal Power Station (TTPS), Thoothukudi, Tamil Nadu, India. p-NP was obtained from Sigma-Aldrich, India. Ammonium peroxydisulfate, aniline, hydrochloric acid (37%), sodium hydroxide and sodium tungstate dihydrate were procured from Merck while ammonium carbonate and hydrogen peroxide were obtained from SD fine chemicals. All the chemicals used were of AR grade and the water used was distilled. The fractional distillation of aniline with zinc dust was carried out to purify it. The initial and final fractions were discarded while the middle fraction containing the colourless aniline boiling constantly at 184 °C was collected and stored in an air-tight bottle.

2.2. Synthesis of single (zeolite-HX) catalyst

Zeolite-NaX was synthesized from acid–treated and purified coal fly ash by alkali fusion followed by hydrothermal treatment as reported in our previous paper (Sudha and Subramanian, 2015). The sodium form of zeolite was then converted to HX form by mixing ammonium carbonate solution (1.0 M) with zeolite-NaX (10 mL/g) in a sealed bottle and shaking well for 10 h. Then the zeolite was filtered, washed and dried overnight at 373 K and then calcinated at 823 K for 4 h in air. In this process first sodium ion in zeolite-NaX was replaced by NH_4^+ ion and zeolite-NaX was converted to zeolite-NH_4X. Then during calcination, NH_3 was liberated from NH_4^+ ion and only H^+ remained in the cavities/pores of zeolite. Hence finally zeolite-HX was synthesized.

2.3. Synthesis of binary photocatalysts

2.3.1 WO_3/zeolite-HX

Tungstic acid H_2WO_4 was first prepared by dissolving sodium tungstate dihydrate (0.330 g) in 1 mL of water followed by addition of 2 mL conc. HCl solution and sonication for 15 min. Then the supernatant liquid was decanted and a yellow-green precipitate of tungstic acid H_2WO_4 was obtained. It was then washed with water to remove any NaCl. Then 1 g of zeolite-HX was added to 1 mL water - tungstic acid mixture and then sonication was applied for 15 min. The mixture was constantly stirred for 24 h. Finally the product was dried (373 K) for overnight and then calcinated (773 K) for 5 h. The dried sample of yellowish-grey color was ground into a fine powder and stored in zip-lock polythene cover with label for further study.

2.3.2 Zeolite-HX/PANI

For the preparation of zeolite-HX/PANI, 750 mg of zeolite-HX was dispersed in 1 mL water and ultrasonicated. Calculated quantity of aniline (4 wt%) and con.HCl were added to zeolite-HX-water dispersion and sonicated. Ammonium peroxodisulfate (APS) was added to the above solution (aniline: APS = 1:1) and the sonication was continued for 15 min. The resultant mixture was kept in a refrigerator overnight for the completion of aniline polymerization. The precipitate was isolated by centrifugation and washed with 1:1 mixture of acetone and distilled water. Finally the product was dried in an oven (393 K) for 4 h. The dried sample was ground into fine powder, stored in air-tight polythene cover and used for characterization and further study.

2.4. Synthesis of ternary (WO_3/zeolite-HX/PANI) photocatalyst

For the preparation of ternary catalyst 750 mg of WO_3/zeolite-HX was taken in the place of zeolite-HX and the remaining procedure was the same as that of zeolite-HX/PANI synthesis (Section 2.3.2). The dried catalyst WO_3/zeolite-HX/PANI was ground into fine powder, stored in air-tight polythene cover and used for characterization and further study.

2.5. Characterization of the synthesized materials

Fourier transform infrared (FTIR) spectra of the powdered samples were recorded using Jasco FTIR spectrophotometer model 410 in the wavenumber range 400-4000 cm^{-1}. X-ray fluorescence (XRF) spectra of the samples were recorded using wavelength dispersive X-ray fluorescence spectroscopy (ASM 100 T). X-ray diffraction (XRD) was recorded for 2θ = 10-80° in a step of 0.05° using PANalytical Expert Pro-MPG instrument with generator set at 30 mA and 40 kV and CuKα radiation (λ = 1.5406 Å). Scanning electron microscope (SEM) images of the samples were taken using Jeol JSM-6390 instrument operating at 20 kV after coating the samples with gold. Diffuse reflectance spectra were recorded with UV-vis spectrophotometer, Shimadzu model UV-2550 against $BaSO_4$. The degradation products of p-NP were analyzed by Shimadzu HPLC coupled with LCMS-2020.

2.6. Photocatalytic process

The photocatalytic activity of the prepared catalyst materials was investigated by following the degradation of p-NP in aqueous solution. In a typical experiment, 200 mL of p-NP solution (20 mg/L) containing 50 mg of the dispersed photocatalyst and H_2O_2, adjusted to required pH value was taken in the photoreactor. The solution was stirred magnetically for 20 min to attain adsorption equilibrium of p-NP with the added catalyst (shown as -20 to 0 min in all relevant figures). From this 2 mL was withdrawn for analysis of p-NP after adsorption equilibrium in dark. Then the p-NP solution was irradiated with visible light from 60 W incandescent tungsten filament lamp (cut off with filter for UV; intensity = 4.61×10^{-4} W/cm^2 at 555 nm measured with 200K Kusam-Meco Luxmeter). A uniform dispersion of photocatalyst particles was ensured by stirring with a magnetic bar and also with air bubbling into the solution, which also provided a constant supply of oxygen. 2 mL of p-NP sample was withdrawn from the reactor solution at regular time intervals (20 min) followed by centrifugation and absorbance measurement at its λ_{max} (UV-vis Spectrometer; Perkin Elmer Lambda 25) in matched 1 cm quartz cuvettes. The experiment was performed for 180 min and repeated twice/thrice with the same material catalyst (after regeneration) and the efficiency was monitored on reuse. The effect of experimental parameters, catalyst loading and pH of the medium on the photodegradation of p-NP was also studied.

3. RESULTS AND DISCUSSION

3.1. FT-IR characterization

The FTIR spectra of the synthesized materials are presented in Figure 1. The absorbance band at 1140-1340 cm^{-1} in Figure 1(a) represents the presence of substituted Al atoms in the tetrahedral forms of silica framework of fly ash (Ojha et al., 2004). The spectrum of zeolite-NaX in Figure 1(b) exhibits absorption at 461, 565, 674 and 754 cm^{-1} and a broad band at 900-1100 cm^{-1}. The band in the region 900-1100 cm^{-1} represents the characteristic asymmetric stretching of Si-O-Al tetrahedral silica framework and Si-O-Si silica framework in the formed zeolite (Amaladhas and Thavamani, 2013). The broad band at 3000-3600 cm^{-1} can be assigned to the asymmetrical stretching of H-O-H or O-H bonds and the bending vibration of the water molecules appears in the region 1590-1750 cm^{-1}. All these characteristic vibrations confirm the formation of zeolite-NaX on alkali treatment of fly ash. The spectrum of zeolite-HX (Figure 1(c)) with very broad band in the region 920-1282 cm^{-1} represents the influence of H^+ on Si-O-Al framework. The two peaks in WO_3/zeolite-HX spectrum (Figure 1(d)) located at 570 cm^{-1} (W-O stretching vibration) and 744 cm^{-1} (W-O-W stretching vibration) (Zou et. al., 2010) were marked, when compared to zeolite-HX; there is a blue shift in the characteristic peaks of zeolite-HX due to WO_3 incorporation into the zeolite pores. In the spectrum of binary zeolite-HX/PANI catalyst shown in Figure 1(e) PANI bands appear at 800 cm^{-1} (1,4 disubstituted benzene) and 1448 cm^{-1} (benzeneoid ring stretching vibration) (Quillard et. al., 1994) which indicate the deposition of PANI on zeolite. In the spectrum of WO_3/zeolite-HX/PANI (Figure 1(f)) bands are located at 786 cm^{-1} (W-O-W stretching vibration) 576 cm^{-1} (W-O stretching vibration) and 1458 cm^{-1} (benzenoid ring stretching vibration). Thus the IR spectra provide evidence for WO_3/zeolite-HX and WO_3/zeolite-HX/PANI materials and confirm their synthesis.

3.2. XRF analysis

The chemical composition of fly ash, acid treated fly ash and zeolite-NaX was determined by XRF spectroscopy. The data are presented in Table 1. Fly ash contains greater than 90% of three major components (SiO_2, Al_2O_3, and Fe_2O_3) combined and less than 5% of calcium and other metal oxides (not given in Table 1), with CaO content of 1.2%. According to the ASTM (American Society for Testing Material) (ASTM, 2005) standard, this fly ash belongs to Sialic type. On acid treatment the metal oxides were removed and calcium oxide content was reduced to 0.81%. On zeolite synthesis from acid treated fly ash, the silica content was considerably reduced while the alumina content was only slightly reduced. Hence the SiO_2 to Al_2O_3 ratio of 2 both for fly ash and acid treated fly ash was reduced to 1.48 for zeolite-NaX (Table 1). This reduction in SiO_2/Al_2O_3 ratio confirms the zeolite product.

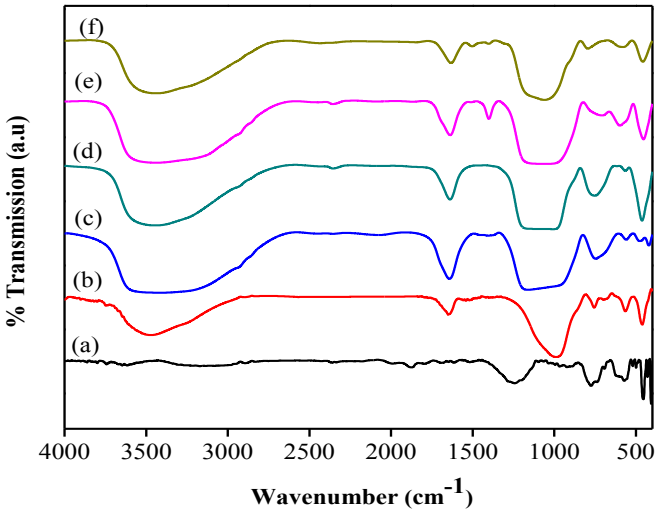

Figure 1. FTIR spectra of (a) fly ash, (b) zeolite-NaX, (c) zeolite-HX, (d) WO_3/zeolite-HX, (e) zeolite-HX/PANI and (f) WO_3/zeolite-HX/PANI.

Table 1. Chemical composition of catalyst materials from XRF analysis.

Materials	% of composition			Si/Al ratio
	SiO_2	Al_2O_3	Fe_2O_3	
Fly ash	58.02	29.90	5.58	1.94
Acid treated fly ash	59.75	29.46	5.23	2.03
Zeolite-NaX	42.76	28.71	5.42	1.48

3.3. XRD analysis

Figure 2(a) and 2(b) display the XRD patterns of fly ash and zeolite-NaX respectively. In Figure 2(a) fly ash shows the diffraction peaks at 2θ = 26.50°, 39.30° and 40.78° (Treacy and Higgins, 2001). The diffraction peaks at 2θ = 15.47°, 23.37°, 26.36°, 31.03° and 51.70° found in Figure 2(b) (JCPDS card No. 89-8604) confirmed the formation of zeolite-NaX crystal (Amaladhas and Thavamani, 2013). The XRD patterns of fly ash and zeolite-NaX contains sharp high intense signals and hence they show crystalline nature of the

two materials. The XRD patterns of WO_3/zeolite-HX material (Figure 2(c)) exhibit broad signal peak at 2θ = 25.33° while the pure WO_3 monoclinic phase has sharp peak at 24.33° (JCPDS Card No. 72-1465) (Katsumata et al., 2013). The slight higher angle shifting in WO_3/zeolite-HX material compared to pure WO_3 indicates the interaction between WO_3 and zeolite faces. Similarly the zeolite-HX/PANI material (Figure 2(d)) exhibits signal at higher 2θ (26.36°) compared to the normal peak position of pristine PANI at 2θ = 25° (Quillard et al., 1994). The higher side shifting also indicates the interaction between PANI and zeolite. Interestingly the WO_3/zeolite-HX/PANI material (Figure 2(e)) shows two signals one at 26° and another at 28.90°. This observation demonstrates the interaction among three components. Thus XRD results not only prove the formation of zeolite from coal fly ash but also indicate the interaction between the components in photocatalysts materials.

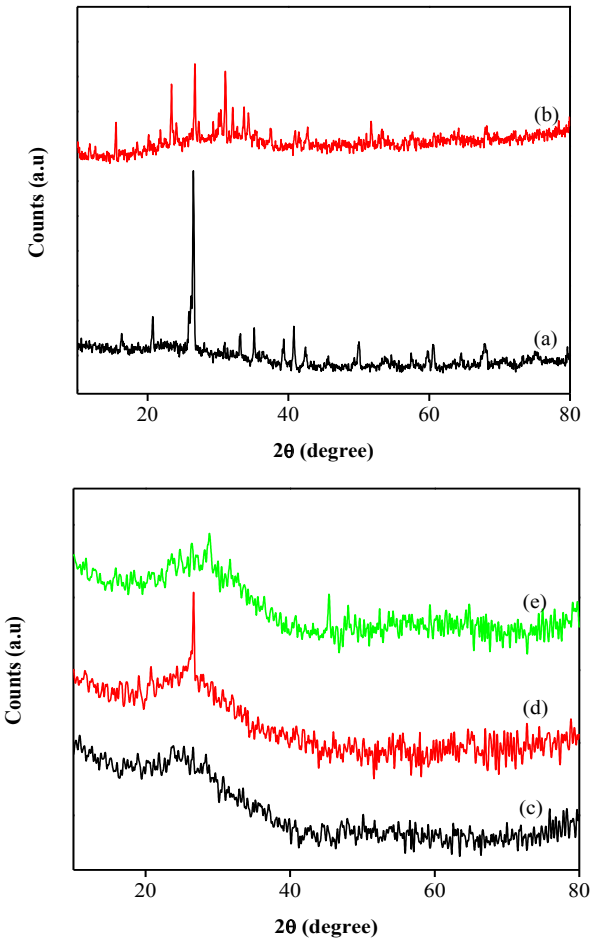

Figure 2. XRD patterns of (a) fly ash, (b) zeolite-NaX, (c) WO_3/zeolite-HX, (d) zeolite-HX/PANI and (e) WO_3/zeolite-HX/PANI.

3.4. SEM and EDX studies

The SEM images of the prepared materials are displayed in Figure 3. All the materials have more or less same morphology. By carefully viewing the lower and higher magnification images, it was observed that the materials have rough surface with approximately spherical particles. The lower magnification images (Figure 3b, d and f) show an array of irregularly shaped and agglomerated secondary particles and the size range was from submicron to few microns. These secondary particles consist of primary nanoparticles observable as white dots/patches in higher magnification images. The rough surface of the particle demonstrates the presence of porous structure.

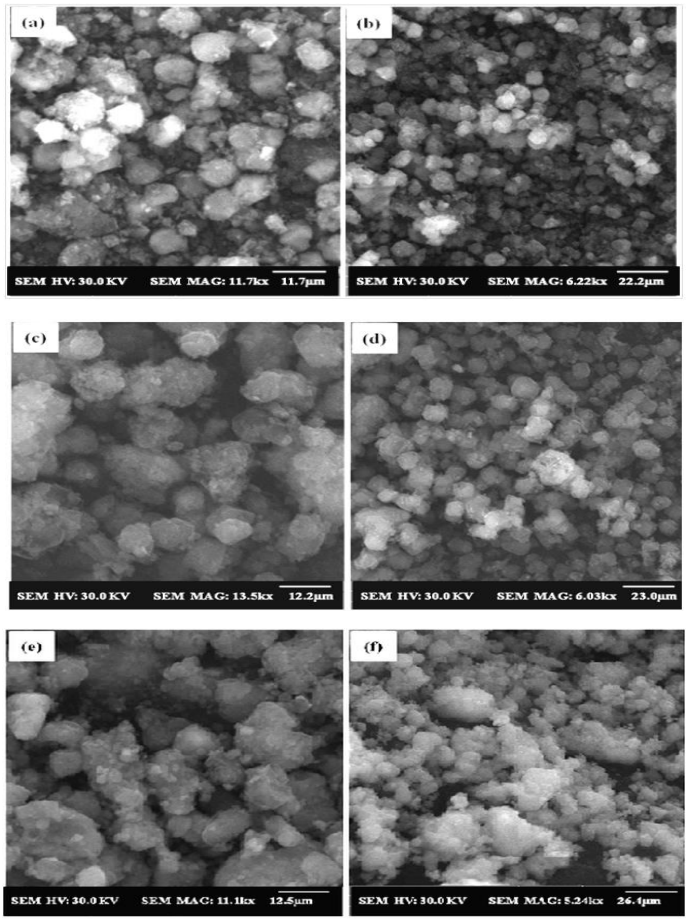

Figure 3. SEM images with higher and lower magnifications in sequence of (a and b) WO_3/zeolite-HX, (c and d) zeolite-HX/PANI and (e and f) WO_3/zeolite-HX/PANI.

The elemental analysis data of SEM EDX given in Table 2 clearly indicate the presence of relevant elements and the chemical composition of the catalyst materials. The EDX data in Table 2 show the presence of W in WO_3/zeolite-HX and PANI in terms of C, N and

Table 2. Elemental composition of the materials from SEM-EDX analysis.

Materials	Elemental (atomic %)							
	Si	Al	W	C	N	Cl	O	Si/Al
WO_3/zeolite-HX	12.1	10.49	1.58	0.00	0.00	0.00	75.78	1.15
Zeolite-HX/PANI	7.66	5.58	0.00	20.41	4.56	0.38	61.42	1.37
WO_3/zeolite-HX/PANI	7.75	6.99	1.21	16.02	4.56	0.92	62.55	1.10

Cl in zeolite-HX/PANI. The WO_3/zeolite-HX/PANI material comprise of both W and elements of PANI. The EDX data thus confirm the loading of WO_3 and/or PANI over zeolite-HX. Furthermore, all the three catalyst materials have Si/Al ratio less than 1.5 in the range of 1.1 to 1.37 and thus have sialic type zeolite mineral phase.

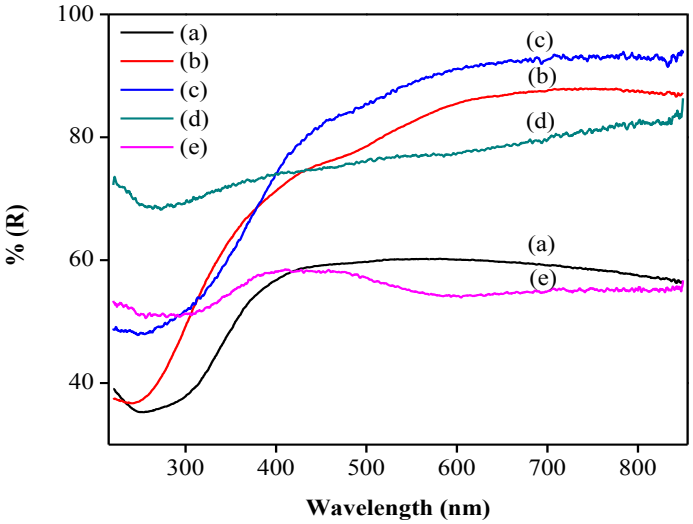

Figure 4. Diffuse reflectance spectra of the photocatalysts (a) fly ash, (b) zeolite-NaX, (c) WO_3/zeolite-HX, (d) zeolite-HX/PANI and (e) WO_3/zeolite-HX/PANI.

3.5. Diffuse reflectance spectral study

Diffuse reflectance spectra (DRS) of the materials are plotted in Figure 4 and the bandgap energy (E_g) values were obtained from the average of both direct and indirect bandgap transition energies. From the spectra (Figure 4a, b and c), it was noticed that fly ash, zeolite-NaX and WO_3/zeolite-HX have clear demarcation between absorbance and non-absorbance regions. But zeolite-HX/PANI and WO_3/zeolite-HX/PANI materials (Figure 4d and e) do not show such demarcation. In other words the latter two materials exhibit light absorption in the entire wavelength region, due to the presence of PANI which extends absorption in the visible and IR regions. Accordingly the band gap energy values (Table 3) have the trend. Zeolite-NaX has the highest value (3.04 eV) while the ternary catalyst has the lowest value (1.62 eV). On incorporating WO_3/PANI into the zeolite, E_g value was reduced considerably. It was inferred that the ternary catalyst has maximum light absorption in the entire visible region followed by binary catalysts (in the decreasing order, zeolite-HX/PANI > WO_3/zeolite-HX) and the zeolite-HX catalyst. This trend in light absorption could reflect in their photocatalytic activities also.

Table 3. Band gap energies of the photocatalysts.

Catalyst	E_g (eV)	λ_{abs} (nm)
Fly ash	2.62	473
Zeolite-NaX	3.04	407
WO_3/zeolite-HX	2.46	500
Zeolite-HX/PANI	1.81	601
WO_3/zeolite-HX/PANI	1.62	765

3.6. Photocatalytic degradation of p-NP

The photocatalytic activity of the bare zeolite-HX, WO_3 and PANI as well as binary and ternary catalysts, WO_3/zeolite-HX, zeolite-HX/PANI and WO_3/zeolite-HX/PANI was studied for the visible light degradation of p-NP. Firstly a preliminary study was performed in order to quantify the efficiencies of the different catalysts. Table 4 compiles the results of degradation efficiencies determined from the experiments performed at the optimal condition (given in the footnote of Table 4). Among the single catalysts, zeolite-HX is the least efficient with miniscule value while WO_3 and PANI, being colored, exhibit relatively better efficiencies. In case of binary catalysts, as anticipated from the DRS results, both the catalysts WO_3/zeolite-HX and zeolite-HX/PANI exhibited remarkably better % degradation, which were about 3-fold of their respective single catalyst values. In the case of ternary catalyst, the % degradation (89%) was twice that of WO_3/zeolite-HX (44.5%) and 1.5 times the value of zeolite-HX/PANI.

Unequivocally all the results reveal that when the catalytic components were coupled in binary form, a 3-fold increase in efficiency and whereas coupled in ternary form a further 1.5/2 fold increase in efficiency could be achieved for the photocatalyst materials. This was possible because when the individual components were coupled in binary or ternary form, they co-operate and co-activate each other constructively exhibiting synergism and thereby they make the p-NP degradation many-fold efficient.

Considering that binary and ternary catalysts exhibit remarkable efficiencies, they were further explored by varying two parameters, namely effect of pH and catalyst dosage on p-NP degradation.

Table 4. Visible light degradation of p-NP over single, binary and ternary catalysts.

Catalysts	p-NP degradation (%)
Zeolite-HX	4.1
WO_3	13.5
PANI (Polyaniline)	22.6
WO_3-zeolite-HX	44.5
Zeolite-HX/PANI	60.1
WO_3/zeolite-HX/PANI	89.2

Reaction condition: [p-NP] = 20 mg/L, catalyst amount = 50 mg, H_2O_2 = 2 mL, pH = 4.0, volume = 200 mL, reaction time = 200 min.

3.6.1. Effect of pH

The solution pH is one of the most important factors in determining the degradation of pollutants. The initial pH of the p-NP solution was adjusted using 0.1M HCl/NaOH solution. The reaction was carried out with acidic pH 4.0, neutral pH 7.3 and alkaline pH 10 keeping the amount of catalyst (50 mg), H_2O_2 (2 mL) and dye concentration (20 mg/L) as constant. Results are presented in Figures 5a - c and Table 5. The alkaline pH 10 of the medium drastically decreases the degradation efficiency of the catalysts while acidic pH 4.0 enhances the degradation as compared to the neutral pH 7.3. As the pK_a of p-NP is 7.16, at acidic pH p-NP exists almost completely in phenolic hydroxyl form, whereas at neutral pH, around 50% exists as phenolic hydroxyl whereas the remaining exists in phenoxide form. At alkaline pH, p-NP exists completely in phenoxide form. Phenolic hydroxyl form is neutral and does not carry any charge while the phenoxide form has negative charge. Since, zeolite framework has negative charge (balanced by counter cations), the electrostatic interaction (particularly at pH 10, negative-negative repulsion) between p-NP and zeolite plays an unfavorable role in the degradation of p-NP. At neutral pH 7.3, since half the amount of p-NP exists in neutral form, it improves the % degradation. At acidic pH 4.0, considering the bulk of p-NP exists in neutral form, there was no electrostatic repulsion/ no inhibition in p-NP degradation, and hence a complete enhancement was possible. Considering all these aspects, pH remains an important factor for degradation of p-NP.

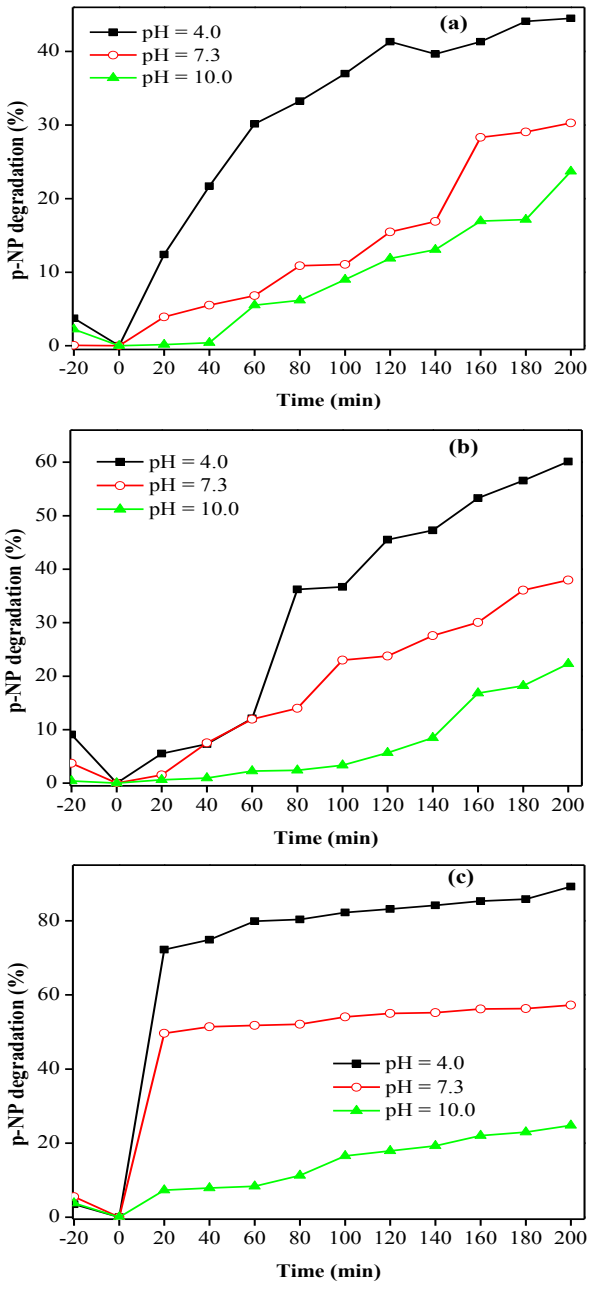

Figure 5. Effect of pH on % degradation of p-NP over (a) WO_3/zeolite-HX, (b) zeolite-HX/PANI and (c) WO_3/ zeolite-HX/PANI (-20 to 0 min – dark adsorption).

3.6.2. Effect of catalyst dosage

The effect of catalyst loading was studied by varying the catalyst dosage from 25 to 100 mg for the reaction solution of volume 200 mL (i.e., 125 – 500 mg/L) maintaining acidic pH and other optimized parameters (dye concentration = 20 mg/L, H_2O_2 = 2 mL) constant. The effect of catalyst dosage on % degradation of p-NP is illustrated in Figures 6(a-c) and in Table 6.

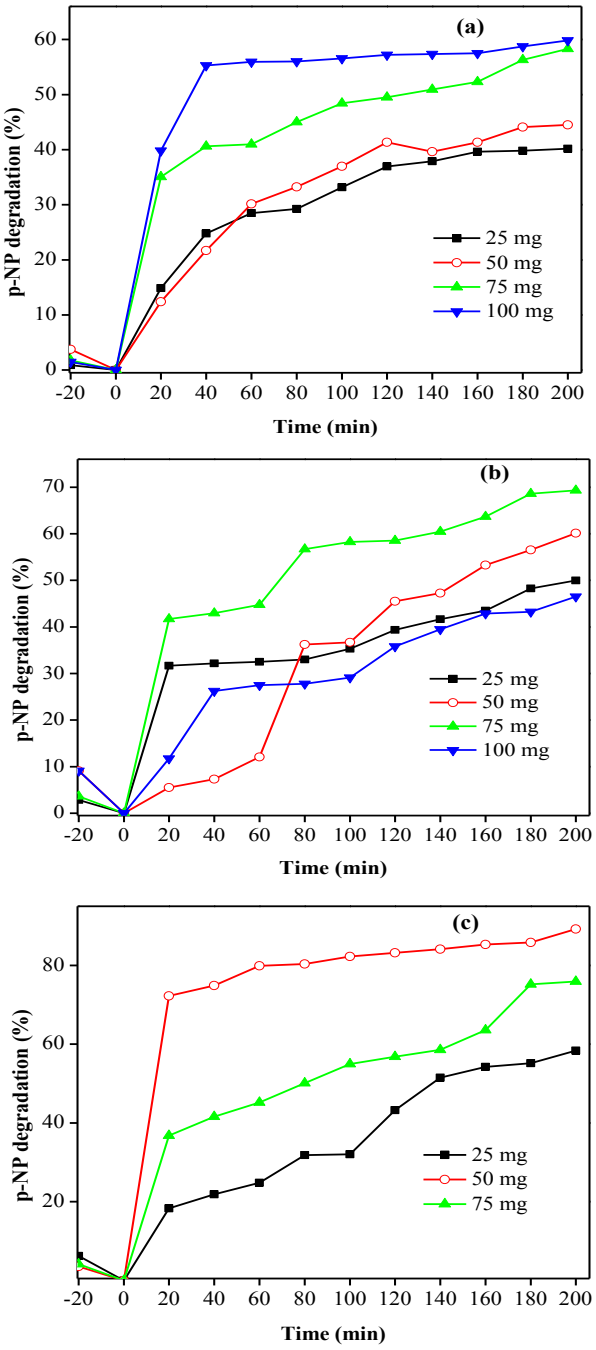

Figure 6. Effect of catalyst dose on % degradation of p-NP over (a) WO_3/zeolite-HX, (b) zeolite-HX/PANI and (c) WO_3/zeolite-HX/PANI (-20 to 0 min – dark adsorption).

Table 5. Effect of pH on % degradation of p-NP.

Catalyst	% degradation at pH		
	4.0	7.3	10
WO_3/zeolite-HX	89.2	53.6	23.0
Zeolite-HX/PANI	60.1	38.0	23.0
WO_3/zeolite-HX/PANI	44.5	30.3	23.7

Reaction condition: [p-NP] = 20 mg/L, catalyst amount = 50 mg, H_2O_2 = 2 mL, volume = 200 mL, reaction time = 200 min.

Table 6. Effect of catalyst dosage on % degradation of p-NP.

Catalyst	% degradation at catalyst dosage (mg/200mL)			
	25	50	75	100
WO_3/zeolite-HX	40.2	44.5	58.3	59.8
Zeolite-HX/PANI	50.0	60.1	69.3	46.5
WO_3/zeolite-HX/PANI	58.4	89.2	75.9	-

Reaction condition: [p-NP] = 20 mg/L, pH = 4, H_2O_2 = 2 mL, volume = 200 mL, reaction time = 200 min.

According to the results, the effect was not uniform for all the three catalysts. In the case of WO_3/zeolite-HX, % degradation of p-NP increases with increase in dosage. Near saturation occurs for 75 mg and 100 mg dosages at reaction time of 180-200 min. For zeolite-HX/PANI, up to 75 mg dosage the % degradation increases but decreases at 100 mg dosage. However, for WO_3/zeolite-HX/PANI the maximum % degradation occurs at lower catalyst dosage, i.e., 50 mg and beyond this there was a decline in % degradation. Hence the optimum catalyst dosage for maximum % degradation of p-NP was 100, 75 and 50 mg for WO_3/zeolite-HX, zeolite-HX/PANI and WO_3/zeolite-HX/PANI catalysts respectively. Obviously this decrease in dosage is the manifestation of efficiency of the catalysts in the increasing order; and particularly the activity enhancement with PANI compared to WO_3. This result could be explained on the basis of light absorption of the respective catalysts (discussed in detail in Section 3.5). Greater the light absorption greater is the efficiency of the catalyst. PANI being dark colored, when coupled to zeolite-HX or WO_3/zeolite-HX imparts color and efficiency. Nevertheless, when such strong light absorbing catalyst was dispersed in reaction solution in larger amount, the catalyst particles lying in frontier region could filter the incident photons and could prevent their penetration in to the solution. Consequently the catalyst in the inner region or bulk of the solution could not absorb photons and

could remain only inactive. Hence an optimal level was necessary.

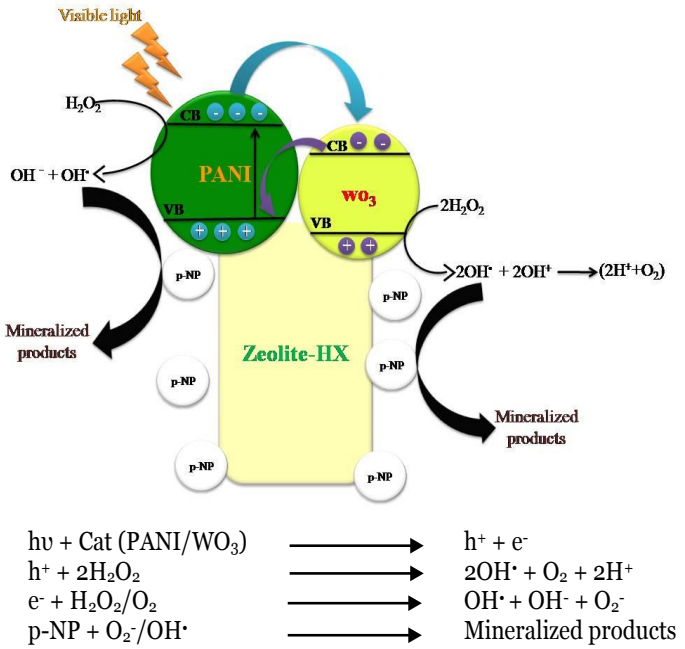

Figure 7. Mechanism of visible light photodegradation of p-NP.

3.6.3. Mechanism of photodegradation of p-NP

As already pointed out and concluded, the binary catalysts (WO_3/zeolite-HX and zeolite-HX/PANI) have efficiency atleast 3-fold higher than those of single catalysts; whereas the ternary catalyst has 2-fold higher efficiency than those of binary catalysts. This catalytic efficiency enhancement arises undoubtedly from synergistic role of the individual components (Figure 7). In single catalyst (WO_3/PANI) e^--h^+ pair excitation occurs on light absorption (Equation 1, Figure 7). H_2O_2/O_2 reacts with h^+_{VB}/e^-_{CB} and produces reactive oxygen species like $OH^\cdot$, $O_2^{\cdot-}$ etc., (Equations 2 and 3). p-NP reacts with these species and undergoes destruction and degradation. In case of binary catalyst similar e^--h^+ pair excitation occurs on light absorption but these charged species are separated efficiently by the zeolite component. Further, being an efficient adsorbent zeolite-adsorbed p-NP readily reacts with h^+_{VB}/e^-_{CB} and undergoes degradation. In ternary photocatalytic system again the same e^--h^+ pair excitation occurs with light absorption but the efficiency of its separation was still greater than the binary. Energetically PANI conduction band is at more negative level (Li et al., 2010; Wang et al., 2015) than the conduction band of WO_3; further PANI has light adsorption in the entire visible and IR region. Hence PANI efficiently absorbs photon and undergoes e^--h^+ excitation. Since the conduction band of PANI is at more negative level, the excited conduction band e^- of PANI was readily transferred to conduction band of WO_3. The charged species arriving WO_3 were further separated with zeolite. Finally they react with H_2O_2/O_2 and produce reactive oxygen species; in turn they react with p-NP and degrade it (Equation 4, Figure 7). A schematic diagram of all these processes and the whole mechanism is shown in Figure 7. This mechanism involves the synergistic role among the three components and explains the highest efficiency of ternary photocatalytic system. A similar mechanism for ternary system chitosan-polypyrrole-TiO_2 has already been proposed and utilized (Murugan and Subramanian, 2015).

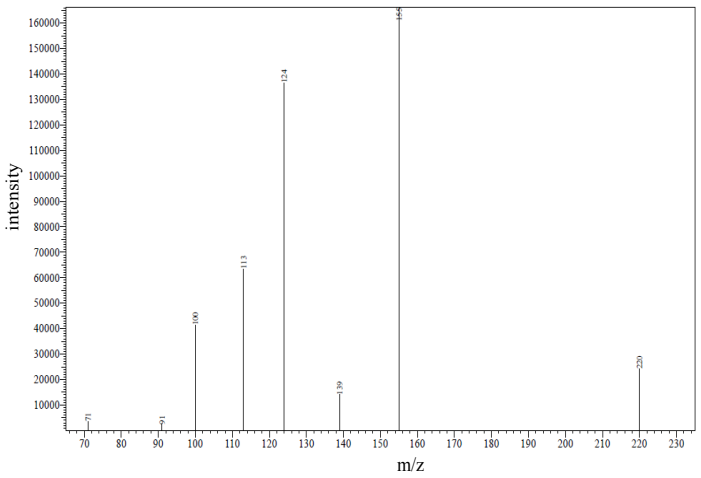

Figure 8. LCMS spectrum of p-NP photodegraded over WO_3/zeolite-HX/PANI for 200 min at pH 4.0.

3.6.4. Analysis of degradation products of p-NP.

Analysis of degradation products was made with LC-MS. The LC-MS spectrum of 200 min degraded p-NP sample over the ternary catalyst at pH 4.0 is shown in Figure 8. The spectrum displays many peaks at m/z values of 139 (parent peak of p-NP), 155 and 220 (both at higher side) and 124, 113, 100, 91 and 71 all at lower side. The low intensity of parent p-NP peak indicates the larger extent of the degradation. The two higher side peaks correspond to 4-nitropyrocatechol/4-nitrohydroquinone and 1,4,5,8-naphthalenetetrol respectively. The lower side peaks show the presence of various fragmented intermediates from p-NP, which include hydroquinone, 1,2,4-benzenetriol and benzoquinone. Based on the LC-MS results the possible mechanistic pathway of p-NP degradation process is illustrated in Figure 9. The p-NP degradation pathway by $OH^\cdot$ oxidation has been well discussed previously (Oturan et al., 2000; Yang et al., 2010; Wang et al., 2011;

Shanthi et al., 2012). The electron-donor property of hydroxyl group in p-NP favors the electrophilic attack of $OH^{\cdot}$ at the ortho- and para-positions of the benzene ring. Attack at ortho-position leads to the formation of 4-nitropyrocatechol. Attack at para-position of p-NP leads to the elimination of nitrite ion from p-NP to yield hydroquinone, which subsequently changes into 1,2,4-benzenetriol and benzoquinone. Subsequently, these intermediates further react with $OH^{\cdot}$ leading to ring cleavage and final formation of carbon dioxide and water, whereas nitrous acid (from nitro group) was oxidized into nitrate ion.

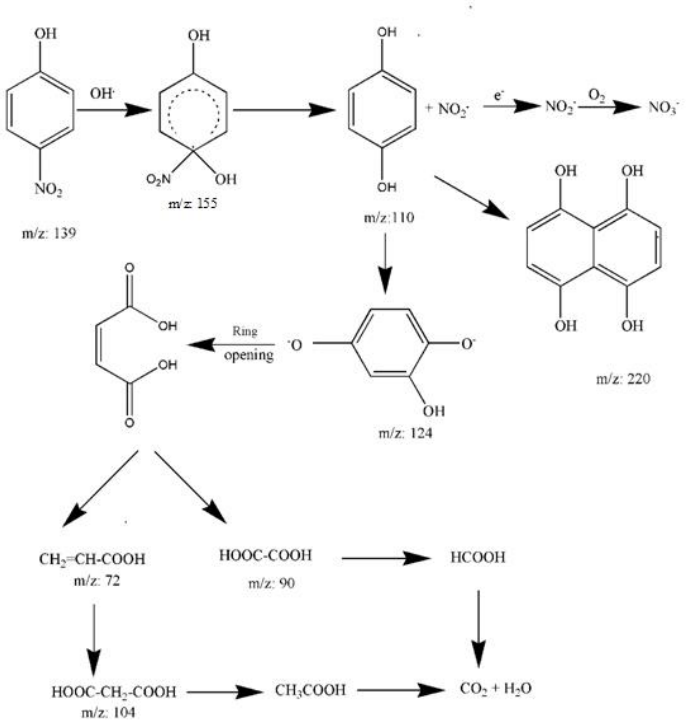

Figure 9. Schematic representation of degradation pathway of p-NP.

4. CONCLUSIONS

The present work is an attempt to design and synthesize single, binary and ternary catalytic systems involving zeolite, WO_3 and conducting PANI. Instrumental (XRF, FTIR, XRD, DRS, SEM and EDX) characterizations reveal the formation of binary and ternary catalyst systems. The p-NP degradation efficiency of the various catalysts was in the following increasing order, single < binary < ternary indicating the synergistic role of the individual components. Plausible mechanism and degradation pathway of p-NP were proposed. Thus the present research indicated that zeolite (from coal fly ash) could be used as an effective support material for photocatalyst and the higher efficiency observed in binary or ternary photocatalyst system could be achieved when the components have intense light absorption and synergistic role.

REFERENCES

Amaladhas, P.T. and Thavamani, S.S. (2013) Synthesis, characterisation and catalytic activity of transition metal complexes of ascorbic acid encapsulated in fly ash based zeolite. Advanced Materials Letters, 4, 688-695.

Abazari, R., Mahjou, A.R., Saghatforoush, L.A. and Sanati, S. (2014) Characterisation and optical properties of spherical WO_3 nanoparticles synthesized via the reverse microemulsion process and their photocatalytic behavior. Materials Letters, 133, 208-211.

ASTM. (2005) Standard specification for coal fly ash and raw or calcined neutral pozzolan for use in concrete (c618-05). In: annual book of ASTM standards, concrete and aggregates, Vol. 04.02. American Society of Testing Materials.

Bi, D. and Xu, Y. (2011) Improved photocatalytic activity of WO_3 through clustered Fe_2O_3 for organic degradation in the presence of H_2O_2. Langmuir, 27, 9359-9366.

Breck, D.W. (1973) Zeolite molecular sieves: Structure, chemistry and use. John Wiley & Sons, New York.

Corma, A. and Garcia, H. (2004) Zeolite based photocatalysts. Chemical Communications, 13, 1443-1459.

Emamul, M.H. (2013) Indian fly-ash: production and consumption scenario. International Journal of Waste Resources, 3, 22-25.

Ganbavle, V.V., Mohite, S.V., Kim, J.H. and Rajpure, K.Y. (2015) Effect of solution concentration on physicochemical and gas sensing properties of sprayed WO_3 thin films. Current Applications in Physics, 15, 84-93.

Katsumata, H., Oda, Y., Kaneco, S. and Tohru, S. (2013) Photocatalytic activity of $Ag/CuO/WO_3$ under visible-light irradiation. RSC Advances, 3, 5028–5035.

Klamrassamee, T., Pavasant, P. and Laosiripojana, N. (2010) Synthesis of zeolite from coal fly ash: Its application as water sorbent. Chemical Engineering Journal, 14, 37-44.

Li, Q., Zang, C. and Li, J. (2010) Photocatalysts and wave-absorbing properties of polyaniline/TiO_2 microbelts composites by in situ polymerization method. Applied Surface Science, 257, 944-948.

Mele, G., Sole, R.D., Vasapollo, G., López, E.G., Palmisano, L. and Schiavello, M. (2003) Photocatalytic degradation of 4-nitrophenol in aqueous suspension by using polycrystalline TiO_2 impregnated with functionalized Cu(II) - porphyrin or Cu(II) – phthalocyanine. Journal of Catalysis, 217, 334-342.

Miyauchi, M. (2008) Photocatalysis and photoinduced hydrophilicity of WO_3 thin films with underlying Pt nanoparticles. Physical Chemistry Chemical Physics, 10, 6258-6265.

More, A.J., Patil, R.S., Dalavi, D.S., Mali, S.S., Hong, C.K. and Gang, M.G. (2014) Electrodeposition of nano-granular tungsten oxide thin films for smart window application. Materials Letters, 134, 298-301.

Murugan, C. and Subramanian, E. (2015) Synthesis and characterization of a novel ternary photoactive chitosan-polypyrrole-TiO_2 system for visible light photocatalytic application. Journal of Advanced Chemical Science, 1, 107-109.

Ojha, K., Pradhan, N.C. and Samanta, A.N. (2004) Zeolite from fly ash: synthesis and characterization. Bulletin of Materials Science, 27, 555–564.

Oturan, M.A., Peiroten, P. and Chartrin, (2000) Complete destruction of p-nitrophenol in aqueous medium by electro-Fenton method. Environmental Science and Technology, 34, 3474-3479.

Querol, X., Alastuey, A., Fernández-Turiel, J. and López-Soler, A. (1995) Synthesis of zeolites from coal fly ash. Fuel, 74, 1226-1231.

Quillard, S., Loarn, G., Lefrant, S. and Macdiarmid, A.G. (1994) Vibrational analysis of polyaniline: a comparative study of leucoemeraldine, emeraldine, and pernigraniline bases. Physics Review B, 50, 12496-12508.

Scheetz, B.E. and Earle, R. (1998) Utilisation of fly ash. Current opinion in solid state and materials science, 3, 510-520.

Shanthi, M., Ginish, E. and Rajamanickam, D. (2012) Photocatalytic degradation of an organic pollutant, benzyl alcohol using an enhanced solar photo-fenton process. Arabian Journal of Chemistry, 5, 2521-2533.

Shinde, S.S., Bhosale, C.H. and Rajpure, K.Y. (2013) Kinetic analysis of heterogeneous photocatalysis: role of hydroxyl radicals. Catalysis Reviews-Science and Engineering, 55, 79-133.

Sudha, G. and Subramanian, E. (2015) Synthesis, characterization and photocatalytic study of cerium oxide/zeolite-NaX catalyst with brilliant green dye degradation. Journal of Advance Chemical Science, 1, 117-120.

Thakare, S.R. (2004) Catalytic degradation of methylene blue by fenton like system: model to the environmental reaction. Journal of Environment Science, 16, 285-287.

Treacy, M.M.J. and Higgins, J.B. (2001) Structure commission of the international zeolite association. 4th Revised Edition, Elsevier publication, New York.

Wang, S. (2008) Application of solid ash based catalysts in heterogeneous catalysis. Environmental Science and Technology, 42, 7055-7063.

Wang, S. and Wu, H. (2006) Environmental-benign utilisation of fly ash as low-cost adsorbents. Journal of Hazardous Materials, 136, 482-501.

Wang, T.C., Lu, N.J., Li. and Wu, Y. (2011) Plasma-TiO_2 catalytic method for high-efficiency remediation of p-nitrophenol contaminated soil in pulsed discharge. Environmental Science and Technology, 45, 9301-9307.

Wang, Y., Xu, J., Zong, W. and Zhu, Y. (2015) Enhancement of photoelectric catalytic activity of TiO_2 film via polyaniline hybridization. Journal of Solid State Chemistry, 184, 1433-1438.

Yang, L., Luo, S., Li, Y., Xiao, Y., Kang, Q. and Cai, Q. (2010) High efficient photocatalytic degradation of p-nitrophenol on a unique Cu_2O/TiO_2 p-n heterojunction network catalyst. Environmental Science and Technology, 44, 7641-7646.

Zou, B.X., Liu, X.X., Diamond, D. and Lau, K.T. (2010) Electrochemical synthesis of WO_3/PANI composite for electrocatalytic reduction of iodate. Electrochimica Acta, 55, 3915-3920.